

Hyperfine interaction in atomically thin transition metal dichalcogenides

I. D. Avdeev¹ and D. S. Smirnov^{1,*}

¹*Ioffe Institute, 194021 St. Petersburg, Russia*

(Dated: October 16, 2018)

Localization of charge carriers in monolayers (MLs) of transition metal dichalcogenides (TMDs) dramatically increases spin and valley coherence times, and, by analogy with other systems, the role of the hyperfine interaction should enhance. We perform theoretical analysis of the intervalley hyperfine interaction in TMD MLs based on the group representation theory. We demonstrate, that the spin-valley locking leads to the helical structure of the in-plane hyperfine interaction. In the upper valence band the hyperfine interaction is shown to be of the Ising type, which can be used for fabrication of the atomically thin quantum dots with the long spin and valley coherence times.

I. INTRODUCTION

Atomically thin TMDs, MX_2 with M being a transition metal (Mo, W) and X being a chalcogen (S, Se, T), represent a new generation of truly two-dimensional structures after graphene [1, 2]. Recently discovered [3, 4], they prove to have unique optical properties [5]: TMD MLs have a direct band gap at the two inequivalent \mathbf{K}_+ and \mathbf{K}_- points of the Brillouin zone [6, 7]. The strong spin-orbit interaction leads to the pronounced spin splitting of the conduction and valence bands [8–10] and results in the valley dependent optical selection rules: σ^\pm light can induce optical transitions only in \mathbf{K}_\pm valleys, respectively [8, 11, 12]. Generally, the optical properties of TMD MLs up to room temperature are determined by the Wannier-Mott excitons with the huge binding energy about 0.5 eV [13–18]. These fascinating optical properties are believed to be potentially useful for a broad range of future applications [19–26].

In recent years the interest shifted towards van der Waals heterostructures based on TMD MLs [21]. However, novel opportunities are also opening in zero-dimensional systems, like quantum dots based on TMD MLs [27, 28]. Such structures seem to be more appropriate for the applications in the optoelectronic devices [29–32] and potentially easier to realize. Indeed, any disorder in 2D structures leads to the localization of the charge carrier wavefunction [33–35], which increases the spin and valley coherence times. In TMD MLs the charge carrier localization can be reached by means of the chemical exfoliation [36–38], lithographic nanopatterning [39], wrinkles [40], homojunctions [41], or defects [42–44].

In TMD MLs the spin and valley degrees of freedom are locked due to the strong spin-orbit coupling and exchange interaction in Coulomb complexes. For excitons, the spin-valley polarization lifetime is limited by the exciton lifetime in the picosecond range. For resident charge carriers this limitation is released. The polarization can be preserved for a few nanoseconds in MoS_2 [45–47], and even longer in WSe_2 [48–50]. Particularly long polarization relaxation times can be obtained for the localized

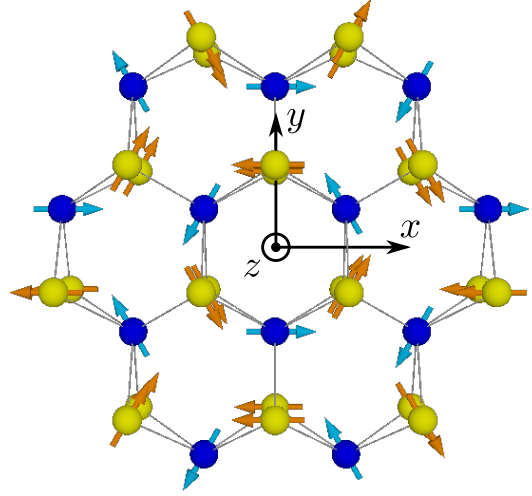


Figure 1. A part of TMD ML and the coordinate frame. The blue and yellow balls show the metal and chalcogen atoms, respectively, with arrows corresponding to the nuclear spins. The orientation of nuclear spins corresponds to the dynamic nuclear polarization induced by the valley pseudospin polarization along x direction.

charge carriers, where the dominant role in the spin and valley dynamics is played by the hyperfine interaction with the host lattice nuclear spins [28, 51].

The microscopic mechanisms of the spin relaxation were studied in very detail in the widespread A_3B_5 semiconductor quantum dots. It was found, that the main source of the spin relaxation in moderate magnetic fields is the hyperfine interaction with the randomly oriented host lattice nuclear spins [51, 52]. We note, that the spin-orbit and the hyperfine interactions have the common relativistic origin, so the pronounced spin-orbit splitting of the conduction and valence bands in TMDs suggests the pronounced hyperfine interaction. It can be particularly strong in the case of the localization in a small area in the vicinity of a point defect. Hence, we assume that the nuclear spin fluctuations are the dominant mechanism of the polarization relaxation for the localized charge carriers in TMD MLs despite the moderate abundance of the nuclear isotopes with nonzero spin.

The spin-valley locking and specific band structure of

* smirnov@mail.ioffe.ru

TMDs can bring new challenges and peculiarities in the hardly explored field of the electron-nuclear interaction in TMD MLs [53]. Any theoretical description of the effects related to the hyperfine interaction is based on the form of the hyperfine interaction Hamiltonian. In this work we derive it from the rigorous symmetry analysis. We also support our results with the microscopic analysis in the tight binding model.

In TMD MLs, the energy degenerate states in the K_+ and K_- valleys are protected by the time reversal symmetry and the vertical mirror reflection symmetry of the structure. The nuclear spin polarization and fluctuations, similarly to an external magnetic field, can break both these symmetries. This results in the splitting and mixing of the degenerate states in the two valleys. Microscopically, the short-range nature of the hyperfine interaction favours the scattering of the charge carriers between the valleys [54]. These effects are also qualitatively discussed in our work on the basis of the form of the hyperfine interaction Hamiltonian.

The paper is organized as follows. In Sec. II we perform the symmetry analysis of the hyperfine interaction. Then, in Sec. III, using the tight binding model we calculate the components of the hyperfine interaction tensors. We provide estimates and discuss the results in Sec. IV. Finally, conclusions are given in Sec. V.

II. SYMMETRY ANALYSIS

A single TMD ML has the honeycomb lattice with one transition metal atom and two chalcogen atoms in the unit cell, see Appendix A. A few unit cells of TMD ML are shown in Fig. 1, where the metal and chalcogen atoms are represented by blue and yellow balls, respectively. The metal atoms lie within the ML plane, (xy) , while the chalcogens are shifted along the z axis in the opposite directions from the ML plane.

We chose the origin of the coordinate frame at the center of the hexagon, formed by the metal and chalcogen atoms [5, 6], as shown in Fig. 1. We also choose the y axis to be oriented towards the nearest pair of the chalcogen atoms. We note, that the caution should be taken to the choice of the coordinate frame origin and axes orientation, when comparing with the results of different authors [7, 55].

The point symmetry of the TMD ML is D_{3h} . This group consists of the horizontal (lateral) reflection plane $\sigma_h \parallel (xy)$, three fold rotation axis $C_3 \parallel z$, three vertical reflection planes $3\sigma_v$, three in-plane two fold rotation axes $3C_2'$ (including y axis), and the combinations $S_3 = \sigma_h C_3$. In total, there are 12 symmetry operations including identity.

The valence and conduction band extrema are located in the two inequivalent K_{\pm} points of the Brillouin zone, see Appendix A for details. The wave vector point symmetry in these valleys is C_{3h} , which is a subgroup of D_{3h} lacking all the elements interchanging the K_+ and K_-

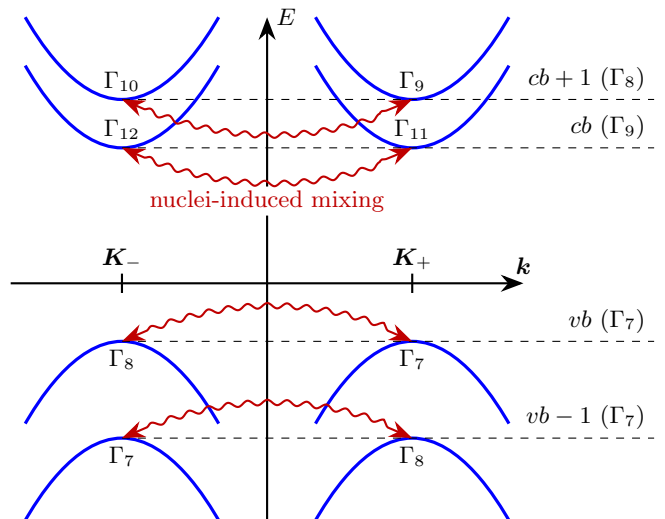


Figure 2. Schematics of the band structure with the red wavy arrows showing the mixing between the energy degenerate states in K_+ and K_- valleys induced by the hyperfine interaction.

valleys.

All the irreducible representations of the C_{3h} group are one dimensional, so that all the electronic states in K_{\pm} valleys are nondegenerate, see the band diagram in Fig. 2. However, the two valleys are related by the time reversal symmetry and their energies coincide, in agreement with the Kramers theorem [56].

We focus our attention on the four bands in the vicinity of the band gap, which we will distinguish by the index $m = cb, cb + 1, vb, vb - 1$, as shown in Fig. 2. The electronic wave function in K_{\pm} valley in the m th band is a Bloch function

$$\Psi_{\pm}^{(m)}(\mathbf{r}) = e^{i\mathbf{K}_{\pm}\mathbf{r}} u_{\pm}^{(m)}(\mathbf{r}), \quad (1)$$

where $u_{\pm}^{(m)}(\mathbf{r})$ is the Bloch amplitude (a spinor). Note, that the functions $\Psi_{+}^{(m)}(\mathbf{r})$ and $\Psi_{-}^{(m)}(\mathbf{r})$ are related by the time reversal symmetry or σ_v reflection.

The nuclear spins weakly break the translation symmetry of the structure and lead to the splitting and mixing of the states in K_+ and K_- valleys. The hyperfine interaction constants are usually of the order of $1 \mu\text{eV}$ [28]. This is much smaller, than the spin-orbit splittings of the conduction and valence bands in TMD MLs, which are of the order of a few tens of meV and a few hundreds of meV, respectively [6, 57]. Therefore, the hyperfine interaction can mix only the states with the same energy, i.e. in the same band, as shown by the wavy arrows in Fig. 2.

The two states in K_+ and K_- valleys can be interpreted as a valley qubit [12, 19, 58, 59]. We introduce the valley pseudospin matrices $\hat{\tau} = (\hat{\tau}_x, \hat{\tau}_y, \hat{\tau}_z)$, see Appendix C, so that the K_{\pm} states correspond to $\tau_z = \pm 1/2$, respectively. Taking into account the form of the electronic wave functions, Eq. (1), the hyperfine interaction

Hamiltonian in the m th band is

$$\hat{\mathcal{H}}_{\text{hf}}^{(m)} = \sum_n e^{-i\hat{\mathbf{K}}\mathbf{R}_n} \hat{\tau} \hat{A}_n^{(m)} \mathbf{I}_n e^{i\hat{\mathbf{K}}\mathbf{R}_n}, \quad (2)$$

where n enumerates the nuclei with the spins \mathbf{I}_n and the two dimensional coordinates \mathbf{R}_n , $\hat{\mathbf{K}} = 2\mathbf{K}_+ \hat{\tau}_z$ is the momentum operator and $\hat{A}_n^{(m)}$ is the tensor of the hyperfine interaction constants. Here we explicitly wrote the two operators (or matrix exponents) $e^{\pm i\hat{\mathbf{K}}\mathbf{R}_n}$, which account for the relative spatial phase shift between $\Psi_+^{(m)}(\mathbf{r})$ and $\Psi_-^{(m)}(\mathbf{r})$. As a result, the tensors $\hat{A}_n^{(m)}$ are independent of the position of the elementary cell in the TMD ML. Moreover, the hyperfine interaction tensors for each pair of chalcogen atoms in the same unit cell are related by the reflection in the horizontal plane, i.e. they are linearly dependent. As a result there are only two independent hyperfine interaction tensors in each band: one with metal and one with chalcogen atoms.

Further symmetry analysis allows one to find the restrictions on the form of the hyperfine interaction tensors. It is most convenient to start the analysis from the C_{3h} group of the wave vector, and then consider the raise of the symmetry up to the D_{3h} , the point symmetry of the structure.

Each single nuclear spin \mathbf{I}_n , with the lateral coordinates $\mathbf{R}_n = (R_{n,x}, R_{n,y})$, breaks the translation symmetry of the structure, which allows for the mixing of the states in the two K_{\pm} valleys. To analyze the hyperfine interaction tensor with the n th nucleus, it is convenient to move the origin of the coordinate frame towards the corresponding nucleus (by the two-dimensional vector \mathbf{R}_n). Upon this nontrivial translation, the irreducible representations of the wavefunctions $\Psi_{\pm}^{(m)}$ change. In Appendix B we show, that for each symmetry operation g of the wave vector point group C_{3h} the matrix of the representation should be multiplied by

$$e^{-i\mathbf{K}_{\pm}(\mathbf{R}_n - g\mathbf{R}_n)}. \quad (3)$$

Sets of these factors form representations, corresponding to the functions

$$f_{\pm}(\mathbf{r}) = e^{-i\mathbf{K}_{\pm}\mathbf{r}} \sum_{\mathbf{a}} \delta(\mathbf{R}_n + \mathbf{a} - \mathbf{r}). \quad (4)$$

Here the sum runs over all translation vectors \mathbf{a} and $\delta(\mathbf{r})$ is the Dirac δ -function. The functions f_{\pm} transform according to the $\Gamma_{2,3}$ ($\Gamma_{3,2}$) representations of the C_{3h} point symmetry group for the n th atom being a metal (chalcogen), respectively. Therefore, representations of the wavefunctions for the two different origins of the coordinate frame are related simply by the multiplication by the representation Γ_2 or Γ_3 .

In Table I we present the irreducible representations of electronic states in C_{3h} group in the bands under study ($cb+1$, cb , vb and $vb-1$). The representations corresponding to the standard choice of the origin of the coordinate frame at the center of the hexagon are well established [5, 60]. The representations corresponding to the

Table I. Spinor irreducible representations of the electronic states in the \mathbf{K}_{\pm} valleys for different choices of the coordinate frame origin: in the center of hexagon (O), at metal atom (M), and between neighboring chalcogen atoms (X) for the C_{3h} point group. The order of bands corresponds to the Mo-based structures.

band	O		M		X	
	\mathbf{K}_+	\mathbf{K}_-	\mathbf{K}_+	\mathbf{K}_-	\mathbf{K}_+	\mathbf{K}_-
$cb+1$	Γ_9	Γ_{10}	Γ_8	Γ_7	Γ_{12}	Γ_{11}
cb	Γ_{11}	Γ_{12}	Γ_7	Γ_8	Γ_{10}	Γ_9
vb	Γ_7	Γ_8	Γ_{10}	Γ_9	Γ_{11}	Γ_{12}
$vb-1$	Γ_8	Γ_7	Γ_{12}	Γ_{11}	Γ_9	Γ_{10}

shifted origin of the coordinate frame can be calculated using the multiplication rules for the C_{3h} group [61], as described above. The two representations, corresponding to the two valleys in the same band, are always conjugate, in agreement with the time reversal symmetry. They join in D_{3h} group in pairs [60, 61]

$$\{\Gamma_8(C_{3h}), \Gamma_7(C_{3h})\} \rightarrow \Gamma_7(D_{3h}), \quad (5a)$$

$$\{\Gamma_{10}(C_{3h}), \Gamma_9(C_{3h})\} \rightarrow \Gamma_8(D_{3h}), \quad (5b)$$

$$\{\Gamma_{11}(C_{3h}), \Gamma_{12}(C_{3h})\} \rightarrow \Gamma_9(D_{3h}). \quad (5c)$$

The order of the representations in the curly brackets corresponds to the standard basis of the representation to the right of the arrow [61]. This rule, together with Table I, allows one to find the irreducible representations of the pairs of wavefunctions $\Psi_{\pm}^{(m)}$ in the D_{3h} point symmetry group with the coordinate frame origin being at \mathbf{R}_n . The results are listed in the second columns of Tables II and III. One can see, that it can be either Γ_7 , or Γ_8 , or Γ_9 . For the rest of the paper all irreducible representation labels will refer to the D_{3h} point group.

The irreducible representations corresponding to the components of the valley pseudospin $\hat{\tau}$ can be found from the decomposition of the squares of the self-conjugate representations found above. The multiplication rules read [61]

$$\Gamma_7 \otimes \Gamma_7 = \Gamma_8 \otimes \Gamma_8 = \Gamma_1 \oplus \Gamma_2 \oplus \Gamma_5, \quad (6a)$$

$$\Gamma_9 \otimes \Gamma_9 = \Gamma_1 \oplus \Gamma_2 \oplus \Gamma_3 \oplus \Gamma_4. \quad (6b)$$

Specifically, in Appendix C we show that for the representations Γ_7 and Γ_8 the valley pseudospin component $\hat{\tau}_z$ transforms according to Γ_2 , while $\hat{\tau}_{x,y}$ form the basis of the representation Γ_5 . For the representation Γ_9 we find, that $\hat{\tau}_z$ again transforms according to Γ_2 , while $\hat{\tau}_x$ and $\hat{\tau}_y$ form the bases of the representations Γ_3 and Γ_4 , respectively.

Now let us turn to the classification of the nuclear spin components. We recall, that we perform the symmetry analysis in the point symmetry group D_{3h} with

the center of transformations chosen at \mathbf{R}_n (a two dimensional atomic coordinate). The nuclear spin of a metal atom, \mathbf{I}_M , is a pseudovector, its components transform according to Γ_2 ($I_{M,z}$) and Γ_5 ($\pm I_{M,x} - iI_{M,y}$) irreducible representations. The two chalcogen atoms at the two-dimensional coordinate \mathbf{R}_n (in the same unit cell) exchange their places under the reflection in the horizontal plane σ_h . So it is useful to introduce the linear combinations of their spins $\mathbf{I}_X = (\mathbf{I}^{\text{up}} + \mathbf{I}^{\text{down}})/2$ and $\Delta\mathbf{I} = (\mathbf{I}^{\text{up}} - \mathbf{I}^{\text{down}})$, where the superscripts ‘‘up’’ and ‘‘down’’ refer to the spins of the atoms above and below (xy) plane, respectively. Under the reflection σ_h the components of \mathbf{I}_X transform in the same way as those of \mathbf{I}_M , while the components of $\Delta\mathbf{I}$ additionally change the sign. Under the reflection in the vertical plane σ_v the components of both \mathbf{I}_X and $\Delta\mathbf{I}$ transform in the same way as those of \mathbf{I}_M . As a result the components $I_{X,z}$ and $\pm I_{X,x} - iI_{X,y}$ belong to Γ_2 and Γ_5 representations, respectively; the component ΔI_z belongs to Γ_3 representation, while the others, ΔI_x and ΔI_y , form the basis of the representation Γ_6 .

Now the symmetry analysis of the hyperfine interaction becomes straightforward. According to the method of invariants the coupling is allowed only between the components of $\hat{\boldsymbol{\tau}}$ and \mathbf{I} , which transform according to the same irreducible representation. For the representations Γ_7 and Γ_8 corresponding to the coordinate \mathbf{R}_n of the n -th nucleus the hyperfine interaction Hamiltonian has the form:

$$\begin{aligned} \mathcal{H}_n^{\Gamma_7, \Gamma_8} &= A_{n,xx} (\hat{\tau}_x \cos \phi_n + \hat{\tau}_y \sin \phi_n) I_{n,x} \\ &+ A_{n,yy} (\hat{\tau}_y \cos \phi_n - \hat{\tau}_x \sin \phi_n) I_{n,y} + A_{n,zz} \hat{\tau}_z I_{n,z}, \end{aligned} \quad (7)$$

where we took into account the phase factors in Eq. (2) $\phi_n = 2KR_{n,x}$ with $K = |\mathbf{K}_{\pm}|$. The absolute values of in-plane hyperfine coupling constants are equal: $|A_{n,xx}| = |A_{n,yy}|$, while their signs can be opposite or the same depending on the representations of the electronic states in K_+ and K_- valleys in the C_{3h} group. Below we focus on the Mo-based structures, as for the W-based structures the results are the same, except for the swap of the band cb with $cb + 1$. Thus one has $A_{xx} = A_{yy}$ for Mo atoms in the cb and for chalcogen atoms in $vb - 1$. By contrast, for Mo atoms in the bands $cb + 1$ and vb and for chalcogen atoms in cb one has $A_{yy} = -A_{xx}$, see Tables II and III.

In the case of the representation Γ_9 the Hamiltonian has the form

$$\begin{aligned} \mathcal{H}_n^{\Gamma_9} &= A_{n,zz} \hat{\tau}_z I_{n,z} \\ &+ A_{n,xz} (\hat{\tau}_x \cos \phi_n + \hat{\tau}_y \sin \phi_n) (I_{n,z}^{\text{up}} - I_{n,z}^{\text{down}}). \end{aligned} \quad (8)$$

Here in the second line $\mathbf{I}_n^{\text{up,down}}$ is the spin of chalcogen atom above (below) (xy) plane, and this term is absent for Mo atoms. The Hamiltonian of this type is relevant for Mo atoms in the band $vb - 1$ and for the chalcogen atoms in the bands vb and $cb + 1$.

One can see, that the component A_{zz} is symmetry allowed for all atoms in all the bands. This means, that the nuclear spin polarization along z lifts the Kramers degeneracy of the bands and splits the energy degenerate states, similarly to an external longitudinal magnetic field. The difference between A_{zz} in the pairs of bands $cb, cb + 1$ and $vb, vb + 1$ is analogous to the longitudinal spin g factor of the charge carriers [62, 63]. The in-plane hyperfine coupling is allowed only for the certain bands and atoms and has the ‘‘helical’’ structure, described by the phase factors in Eqs. (7) and (8). In particular, from Eq. (7) one can see, that the coupling coefficients between the valley pseudospin components and nuclear spin components periodically depend on the atomic coordinates. Moreover, the hyperfine interaction can be noncollinear, see the second line in Eq. (8). The coupling between the in-plane valley pseudospin components and out-of-plane nuclear spin components give rise to a number of interesting phenomena for localized charge carriers in TMD MLs [64].

The relations described above are strict and follow only from the symmetry analysis. The same results apply also for any substitutional impurity in TMD MLs. Below we obtain additional restrictions on the components of the hyperfine interaction tensors from the microscopic analysis using the tight binding model. The results of the microscopic analysis are summarized in the Tables II and III and are in full agreement with the symmetry analysis performed in this section.

III. TIGHT BINDING MODEL

The Hamiltonian of the hyperfine interaction with the nuclei has the form

$$\hat{\mathcal{H}}_{\text{hf}} = \sum_n 2\mu_B \mu_I^{(n)} \mathbf{I}_n \left[\frac{8\pi}{3} \hat{\mathbf{s}} \delta(\mathbf{r}_n) + \frac{\hat{\mathbf{l}}_n}{r_n^3} - \frac{\hat{\mathbf{s}}}{r_n^3} + 3 \frac{\mathbf{r}_n (\hat{\mathbf{s}} \mathbf{r}_n)}{r_n^5} \right]. \quad (9)$$

Here μ_B is the Bohr magneton, $\mu_I^{(n)} = g_I^{(n)} \mu_N$ is the nuclear magnetic moment with $g_I^{(n)}$ and μ_N being the nuclear g -factors and the nuclear magneton respectively, \mathbf{r}_n is the electron distance to the n th nucleus (being a three dimensional vector), $\hat{\mathbf{l}}_n = -i[\mathbf{r}_n \times \nabla]$ is the electron angular momentum, and \mathbf{s} is the electron spin operator. The first term in square brackets in Eq. (9) describes the Fermi contact interaction, which vanishes for all atomic orbitals except for the s -type. The other terms describe magnetic dipole-dipole interaction.

The hyperfine interaction of charge carriers with the host lattice nuclei is a short range interaction [28, 65], so it can be conveniently studied within the tight binding approximation. For the sake of simplicity, we limit ourselves with d -orbitals at the metal atoms (thus neglecting s -orbitals [66]) and p -orbitals at the chalcogen atoms [6, 55]. In this basis the orbital part of the wavefunction is even with respect to the reflection σ_h

Table II. Irreducible representations of the wavefunctions in the point symmetry group D_{3h} with the center of transformations at a metal atom and the components of the hyperfine interaction tensor with the metal atoms \hat{A}^M .

band	irrep(M)	A_{xx}^M/A^M	A_{yy}^M/A^M	A_{zz}^M/A^M
$cb+1$	Γ_7	2/7	-2/7	-4/7
cb	Γ_7	2/7	2/7	4/7
vb	Γ_8	0	0	24/7
$vb-1$	Γ_9	0	0	32/7

($z \rightarrow -z$). As a result the Knight fields acting on the two chalcogen atoms in the same unit cell are the same, and the component A_{xz} vanishes in this model. We note, that admixture of d -orbitals odd along z axis at the chalcogen atoms [60] can provide nonzero coupling between τ_x and ΔI_z and make the hyperfine interaction anisotropic. The similar effect takes place for the holes in GaAs quantum dots with C_{3v} symmetry [67].

Bearing in mind the irreducible representations of the point groups with the centers of transformations at a metal atom or between neighboring chalcogen atoms (Table I), one can find the explicit form of the Bloch amplitudes straight from the tight-binding model [6, 55]. For Mo-based structures they read

$$u_{\pm}^{cb+1}(\mathbf{r}) = [\pm \mathcal{D}_0(\mathbf{r}) \pm \mathcal{P}_{\mp 1}(\mathbf{r})] |\downarrow / \uparrow\rangle, \quad (10a)$$

$$u_{\pm}^{cb}(\mathbf{r}) = [\mp \mathcal{D}_0(\mathbf{r}) \mp \mathcal{P}_{\mp 1}(\mathbf{r})] |\uparrow / \downarrow\rangle, \quad (10b)$$

$$u_{\pm}^{vb}(\mathbf{r}) = [\mathcal{D}_{\pm 2}(\mathbf{r}) + \mathcal{P}_{\pm 1}(\mathbf{r})] |\uparrow / \downarrow\rangle, \quad (10c)$$

$$u_{\pm}^{vb-1}(\mathbf{r}) = [\mathcal{D}_{\pm 2}(\mathbf{r}) + \mathcal{P}_{\pm 1}(\mathbf{r})] |\downarrow / \uparrow\rangle. \quad (10d)$$

Here the functions $\mathcal{D}_{m_z}(\mathbf{r})$ and $\mathcal{P}_{m_z}(\mathbf{r})$ ($m_z = 0, \pm 1, \pm 2$) denote the Bloch amplitudes formed by the d and p atomic orbitals at metal and chalcogen atoms respectively. In the vicinity of the n th nucleus the orbital wavefunction has the form

$$\mathcal{R}(\mathbf{r}_n) = R_n(\mathbf{r}_n) Y_{lm_z}(\theta, \phi), \quad (11)$$

where the spherical harmonics $Y_{lm_z}(\theta, \phi)$ with $l = 1, 2$ correspond to the functions \mathcal{P}_{m_z} and \mathcal{D}_{m_z} , respectively. The radial parts of the wavefunctions in Eq. (11) are normalized as

$$\int_0^{\infty} R_n^2(r) r^2 dr = 1. \quad (12)$$

Each pair of functions (10a)–(10d) forms the basis of an irreducible representation of the group D_{3h} , and the two corresponding functions belong to the conjugated irreducible representations of the group C_{3h} , in agreement

Table III. Irreducible representations of the wavefunctions in the point symmetry group D_{3h} with the center of transformations between two neighboring chalcogen atoms and the components of the hyperfine interaction tensor with the chalcogen atoms \hat{A}^X .

band	irrep(X)	A_{xx}^X/A^X	A_{yy}^X/A^X	A_{zz}^X/A^X
$cb+1$	Γ_9	0	0	-8/5
cb	Γ_8	-6/5	6/5	-12/5
vb	Γ_9	0	0	8/5
$vb-1$	Γ_8	-6/5	-6/5	12/5

with Eq. (5). We also mention, that in Ref. 28, where the hyperfine interaction was studied from the first principles, the expression for u_{\pm}^{vb} is different, which results in some discrepancies with our results.

Taking into account the explicit form of the wave functions, Eq. (10), additional symmetry restrictions can be obtained for the hyperfine interaction tensors. Indeed, the Hamiltonian (9) can not change the total electron angular momentum $f_z = m_z + s_z$ by more than 1 [68]. The Γ_9 representation corresponds to $f_z = \pm 3/2$, so these states can not be mixed by the hyperfine interaction. In this case the components A_{xx} and A_{yy} vanish, in agreement with the general symmetry arguments. Additionally, the wavefunctions at the metal atoms in the upper valence band, vb , have the total angular momenta $f_z \pm 5/2$, hence $A_{xx} = A_{yy} = 0$, see Table II. As a result the hyperfine interaction in the upper valence band is purely of the Ising type.

The calculation of the matrix elements of the Hamiltonian (9) with the wavefunctions described by Eqs. (10) and (11) yields the relation between the in-plane and out-of-plane components of the hyperfine interaction tensors and their signs. These results are summarized in the last three columns in Tables II and III. One can see, that $|A_{zz}| = 2|A_{xx}|$, whenever A_{xx} is nonzero. The absolute values of the hyperfine interaction constants in Tables II and III are determined by

$$A^{M,X} = 2\mu_B \mu_I^{M,X} \int_0^{\infty} \frac{R_{M,X}^2(r)}{r} dr, \quad (13)$$

where M and X stand for the metal and chalcogen atoms, respectively. Importantly, one can see, that $A^{M,X} > 0$, so Tables II and III yield the overall signs of the hyperfine interaction constants. In particular, the sign of A_{zz} can be both positive and negative in different bands.

IV. DISCUSSION

In TMDs not all the metal and chalcogen isotopes have nonzero nuclear spins. The ones with nonzero nuclear spins are listed in Table IV together with their abundances (ν) and spins (I). One can see, that less than a half of atoms of each type have nonzero spins.

The values of the hyperfine interaction constants (A) can be calculated using atomistic approaches, for example DFT [28, 69, 70]. The orbitals \mathcal{D}_{m_z} at molybdenum and tungsten are related mainly to the $4d$ and $5d$ atomic orbitals, respectively, while the orbitals \mathcal{P}_{m_z} are related to the $3p$, $4p$ and $5p$ atomic orbitals at sulfur, selenium and tellurium, respectively. The estimations for the hyperfine coupling constants can be obtained from the corresponding values known for the free atoms [71], see Table IV. As one could expect, separately for metal and chalcogen atoms, the heavier is the atom the stronger is the hyperfine interaction. The fact that the interaction with nuclei is stronger for the chalcogen atoms than for the metal atoms is related to the fact, that p orbitals correspond to the smaller angular momentum and are more localized at the nuclei, than d orbitals. As a result the hyperfine interaction is most pronounced for tellurium atoms. We note, that the spin-orbit splitting of the conduction and valence bands in TMD MLs qualitatively obeys the same rules. This is related to the common relativistic origin of the two effects.

It is instructive to compare the hyperfine interaction parameters with those in the well studied bulk semiconductor GaAs. In GaAs the spin-orbit splitting of the valence band is about 330 meV [72], which approximately equals to the splitting of the two uppermost valence bands in TMD MLs. The hyperfine interaction constants in the valence band of GaAs are of the order of 10 μeV [73, 74], which is comparable to those in TMDs. Contrary, the hyperfine interaction in the conduction band of GaAs is an order of magnitude stronger due to s type of the Bloch amplitudes [75, 76]. Hence the hyperfine interaction of electrons in TMD MLs is much weaker, than in GaAs.

The most important consequences of the hyperfine interaction are the valley and spin relaxation of localized charge carriers and the dynamic nuclear spin polarization. In accordance with the classical model of Merkulov, Efros and Rosen [77] the spin relaxation in zero magnetic field consists of two stages. In the first stage, the charge carrier spin precesses in the static fluctuation of the Overhauser field \mathbf{B}_N , while the nuclear spin dynamics can be neglected. During this stage the initial spin polarization

Table IV. Properties of the isotopes of M and X atoms with nonzero spin.

	M	ν (%)	I	A (μeV)
Mo	95	15.92	5/2	0.57
	97	9.55	5/2	
W	183	14.31	1/2	0.64
	186	28.43	3/2	
S	33	0.76	3/2	0.75
Se	77	7.63	1/2	3.9
Te	123	0.89	1/2	8.3
	125	7.07	1/2	

along z axis decreases on average by a factor f . In the second stage, the nuclear spin dynamics comes into play, and the charge carrier spin relaxes to zero at parametrically longer timescale.

For the isotropic hyperfine interaction (e.g. when the Fermi contact interaction dominates), the factor f equals to 1/3 [77]. In case of TMD MLs the hyperfine interaction is anisotropic. The hyperfine interaction anisotropy can be described by the parameter λ , which is determined by the relations

$$\lambda^2 = \frac{\langle B_{N,z}^2 \rangle}{\langle B_{N,x}^2 \rangle} = \frac{\langle B_{N,z}^2 \rangle}{\langle B_{N,y}^2 \rangle}, \quad (14)$$

where the angular brackets denote the time or ensemble averaging. Hereafter we assume that the nuclear spins are (i) independent of each other, (ii) randomly oriented, and (iii) the number of nuclear spins in the localization area is large. Provided the valley pseudospin is initially oriented along z , it decreases due to the precession in \mathbf{B}_N by a factor [51]

$$f(\lambda) = \langle B_{N,z}^2 / B_N^2 \rangle = \begin{cases} \frac{\lambda^2 (\sqrt{\lambda^2 - 1} - \arctan \sqrt{\lambda^2 - 1})}{(\lambda^2 - 1)^{3/2}}, & \lambda > 1 \\ 1/3, & \lambda = 1 \\ \frac{\lambda^2 (-\sqrt{1 - \lambda^2} + \operatorname{arctanh} \sqrt{1 - \lambda^2})}{(1 - \lambda^2)^{3/2}}, & \lambda < 1 \end{cases}. \quad (15)$$

Particularly, one can see, that $f(1) = 1/3$ and $f(0) = 0$, as expected.

As one can see from Tables II and III, in the lower conduction band $\lambda = 2$, and

$$f(2) = \frac{4}{27} (9 - \sqrt{3}\pi) \approx \frac{1}{2}. \quad (16)$$

Therefore, the valley polarization of localized charge carriers in this band decreases approximately two times in a few tens of nanoseconds before decaying to zero at longer times. A small admixture of s -type orbitals at metal atoms [7] can slightly change this ratio.

The most interesting situation in TMD MLs takes place in the upper valence band. Here, as follows from Tables II and III, $\lambda = \infty$ and $f = 1$. This describes the situation, when the relaxation of the spin z component is absent because of the Ising type of the hyperfine interaction. For chalcogen atoms this is the symmetry requirement, while for metal atoms this results from $\mathcal{D}_{\pm 2}$ atomic orbitals, which can not be mixed by the hyperfine interaction Hamiltonian (9). Therefore, one should expect the longest valley coherence times for localized holes in TMD MLs.

At long timescales the valley relaxation of localized holes can be related with (i) two phonon processes [78–80], (ii) single phonon processes in combination with the hyperfine interaction [81], or (iii) mixing of the energy

degenerate states by the localization potential [82–84]. In the latter case, the localization potential should be atomically sharp, e.g. an impurity. Otherwise, the degree of mixing of the two valleys is proportional to the ratio α of the lattice constant and the localization length. This situation is similar to the one described above with effective degree of the hyperfine interaction anisotropy $\lambda_{\text{eff}} \sim 1/\alpha$.

Similarly, the dynamic nuclear spin polarization is inefficient in the upper valence band of TMD MLs, while in all the other bands it can be significant. Interestingly, due to the difference of the valleys wavevectors, \mathbf{K}_+ and \mathbf{K}_- , the Hamiltonian of the hyperfine interaction, Eqs. (7) and (8), contains additional phase factors, that “rotate” nuclear spins. An example of nuclear spin polarization distribution for $\boldsymbol{\tau} \parallel \mathbf{x}$ is given in Fig. 1, where one can clearly see the “helical” structure of nuclear spin polarization. This situation can be realized under linearly polarized excitation of TMD MLs. Importantly, the in-plane dynamical nuclear spin polarization is nonuniform in space. Despite the nuclear spin ordering, on average, the nuclear spin polarization is absent, which is analogous to antiferromagnetic spin state [85]. Accordingly, the uniform nuclear spin polarization in (xy) plane, does not lead to the splitting or mixing of the valleys because of the difference of Bloch wavevectors \mathbf{K}_+ and \mathbf{K}_- .

Finally, we note, that in the case of the charge carrier localization in a two dimensional structure the many-body nuclear spin effects, such as nuclear spin self-polarization [86, 87] and formation of nuclear spin polaron [88, 89] can be pronounced. These effects can be used to additionally increase the valley pseudospin relaxation time and to realize robust control of its orientation, similarly to magnetic skyrmions [90, 91].

V. CONCLUSION

Using the symmetry and microscopic analysis we have obtained explicit expressions for the hyperfine interaction tensors in TMD MLs, Tables II and III. Particularly, the valley pseudospin flips induced by the nuclei can take place only for the total electron angular momentum $f_z = \pm 1/2$ at the corresponding atom. This restriction leads to the Ising type of the hyperfine interaction in the upper valence band and favours long valley pseudospin relaxation times of localized holes. Dynamic nuclear spin polarization in TMD MLs is shown to be of the ferromagnetic or antiferromagnetic (“helical”) type for out-of- or in-plane valley pseudospin polarization, respectively.

ACKNOWLEDGMENTS

We thank Q. Tong, W. Yao, and M. M. Glazov for stimulating and useful discussions and acknowledge the Basis Foundation. This work was supported by

the Government of the Russian Federation (contract # 14.W03.31.0011 at the Ioffe Institute of RAS).

Appendix A: Summary of TMD ML structure

Here we present a brief summary of the TMD ML geometry and the choice of the real and reciprocal lattices bases.

A single TMD ML has the honeycomb lattice with the two dimensional translation vectors $\mathbf{a}_1 = a_0(1, 0)$ and $\mathbf{a}_2 = a_0(1/2, \sqrt{3}/2)$, where a_0 is the lattice constant. The choice of the coordinate frame is described in Sec. II. The metal atoms lie within the ML plane (xy) , while the chalcogen atoms are shifted from the plane along and opposite to z axis. The position of the metal atom in the elementary cell is $\boldsymbol{\tau} = a_0/2(1, 1/\sqrt{3})$, and the two chalcogen atoms are located above and below the point $-\boldsymbol{\tau}$.

The reciprocal lattice is determined by the basis vectors $\mathbf{b}_1 = 2\pi/a_0(1, -1/\sqrt{3})$ and $\mathbf{b}_2 = 2\pi/a_0(0, 2/\sqrt{3})$. The extremes of the conduction and valence bands are located at the two inequivalent corners of the hexagonal Brillouin zone, i.e. in $\mathbf{K}_{\pm} = 2\pi/a_0(\pm 2/3, 0)$ valleys.

Appendix B: Shift of point symmetry group transformations center

For the symmetry analysis, described in Sec II, it is necessary to find the irreducible representations of the electronic states for the choices of the point symmetry origins at the $\pm\boldsymbol{\tau}$ points. Here we present a formalism, which solves the problem. It can also be easily generalized for the other problems in physics of multivalley semiconductors.

Let us consider a spatial group $G_{\mathbf{k}}$ of the wave vector $\mathbf{k} = \mathbf{K}_{\pm}$. Further, let us assume, that this group is symmorphic, as in the case of TMD MLs. Let T be the translation subgroup. Then the quotient group $P_{\mathbf{k}} = G_{\mathbf{k}}/T$, being the set of rotations $\{R\}$, is the corresponding point group. By definition, for each R [92]

$$R\mathbf{k} = \mathbf{k} + \mathbf{b}, \quad (\text{B1})$$

where \mathbf{b} is a reciprocal lattice vector (or zero vector).

Now consider a set of the Bloch wave functions $\{\psi_n\} = \{e^{i\mathbf{k}\mathbf{r}} u_n(\mathbf{r})\}$, with $u_n(\mathbf{r})$ being the Bloch amplitude, that forms the basis of an irreducible representation D of the point group $P_{\mathbf{k}}$. Note, that in case of TMD ML, all the irreducible representations are one dimensional, but here we consider a general situation. The wave functions transform under the action of R as

$$R\psi_n = \sum_{n'} \psi_{n'} D_{n'n}(R). \quad (\text{B2})$$

where $\hat{D}(R)$ are the matrices of the irreducible representation D .

Table V. From left to right: the bands; C_{3h} irreducible representations of the electronic states in \mathbf{K}_{\mp} valley with the transformations center at the midpoint of the hexagon and at a metal atom (M); the irreducible representations in D_{3h} group and the basis functions (see Table VII); the form of the hyperfine interaction Hamiltonian.

band	C_{3h}		C_{3h}, M		D_{3h}, M			H_{hf}
	\mathbf{K}_-	\mathbf{K}_+	\mathbf{K}_-	\mathbf{K}_+	irrep	\mathbf{K}_-	\mathbf{K}_+	
$cb+1$	Γ_{10}	Γ_9	Γ_7	Γ_8	Γ_7	ψ_2^7	ψ_1^7	H_-
cb	Γ_{12}	Γ_{11}	Γ_8	Γ_7	Γ_7	ψ_1^7	ψ_2^7	H_+
vb	Γ_8	Γ_7	Γ_9	Γ_{10}	Γ_8	ψ_2^8	ψ_1^8	H_-
$vb-1$	Γ_7	Γ_8	Γ_{11}	Γ_{12}	Γ_9	ψ_1^9	ψ_2^9	H_z

We introduce the point group P'_k with the transformations center shifted by a vector \mathbf{t} as

$$P'_k = \hat{\mathbf{t}} P_k \hat{\mathbf{t}}^{-1}, \quad (\text{B3})$$

where $\hat{\mathbf{t}}$ denotes the translation operator. Note, that generally \mathbf{t} is not a translation vector. The elements g' of P'_k have the form

$$g' = (R|\mathbf{t} - R\mathbf{t}), \quad (\text{B4})$$

being the rotation R with the subsequent shift by the vector $\mathbf{t} - R\mathbf{t}$.

For TMD ML for $\mathbf{t} = \pm\boldsymbol{\tau}$, the vector $\mathbf{t} - R\mathbf{t}$ is a translation vector for each R (see Appendix A), because there are only one metal atom and one pair of chalcogen atoms in the primitive cell. Once this condition is satisfied, one can show that the set $\{e^{-i\mathbf{k}(\mathbf{t}-R\mathbf{t})}\}$ forms a one dimensional representation $D_{\mathbf{t}}$ of the group P_k .

To prove this statement let us consider the two rotations $R_1, R_2 \in P_k$ and the corresponding translation vectors

$$\boldsymbol{\alpha}_{1,2} = \mathbf{t} - R_{1,2}\mathbf{t}. \quad (\text{B5})$$

Since the scalar product is invariant under rotations $\mathbf{k}R_1\boldsymbol{\alpha}_2 = (R_1^{-1}\mathbf{k})\boldsymbol{\alpha}_2$, and

$$e^{i\mathbf{k}(\boldsymbol{\alpha}_2 - R_1\boldsymbol{\alpha}_2)} = 1$$

by the definition of P_k , see Eq. (B1). From this relation, using Eq. (B5), we readily obtain

$$e^{-i\mathbf{k}(\mathbf{t}-R_1\mathbf{t})} e^{-i\mathbf{k}(\mathbf{t}-R_2\mathbf{t})} = e^{-i\mathbf{k}(\mathbf{t}-R_1R_2\mathbf{t})},$$

which proves the multiplication rule, and thus the statement.

Therefore, the set of the functions $\{\psi_n\}$, which transforms according to Eq. (B2), forms the basis of a representation

$$D' = D \otimes D_{\mathbf{t}}, \quad (\text{B6})$$

of the point group P'_k , where $D_{\mathbf{t}}(R) = e^{-i\mathbf{k}(\mathbf{t}-R\mathbf{t})}$, in agreement with Eq. (3).

Table VI. From left to right: the bands; C_{3h} irreducible representations of the electronic states in \mathbf{K}_{\mp} valley with the transformations center at the midpoint of the hexagon and between neighboring chalcogen atoms (X); the irreducible representations in D_{3h} group and the basis functions (see table VII); the form of the hyperfine interaction Hamiltonian.

band	C_{3h}		C_{3h}, X		D_{3h}, X			H_{hf}
	\mathbf{K}_-	\mathbf{K}_+	\mathbf{K}_-	\mathbf{K}_+	irrep	\mathbf{K}_-	\mathbf{K}_+	
$cb+1$	Γ_{10}	Γ_9	Γ_{11}	Γ_{12}	Γ_9	ψ_1^9	ψ_2^9	H_z
cb	Γ_{12}	Γ_{11}	Γ_9	Γ_{10}	Γ_8	ψ_2^8	ψ_1^8	H_-
vb	Γ_8	Γ_7	Γ_{12}	Γ_{11}	Γ_9	ψ_2^9	ψ_1^9	H_z
$vb-1$	Γ_7	Γ_8	Γ_{10}	Γ_9	Γ_8	ψ_1^8	ψ_2^8	H_+

In the \mathbf{K}_- (\mathbf{K}_+) valley of a TMD ML, $D_{\boldsymbol{\tau}}$ is the $\Gamma_{2(3)}$ representation and $D_{-\boldsymbol{\tau}}$ is the representation $\Gamma_{3(2)}$ of the C_{3h} point group. The multiplication of the representations allows us to find the irreducible representations of the wave functions with different centers of transformations. The representations of D_{3h} group are summarized in Tables II and III, while the representation of C_{3h} group are given in Tables V and VI. The correspondence between them is established using the compatibility Table VII.

Appendix C: Pseudospin operators

Here we explicitly construct the pseudospin operators in the dyadic form, which act in the valley pseudospin 2×2 space. The bases of the representations are chosen in agreement with Ref. 61.

It follows from Eq. (6a), that in the corresponding cases one can construct the valley pseudospin operators belonging to Γ_2 and Γ_5 representations. We denote the standard bases of Γ_7 (Γ_8) representation as $\mathbf{u} = (|1\rangle, |2\rangle)$ and $\mathbf{v} = (-\langle 2|, \langle 1|)$. These two bases can be obtain one from another performing the time reversal with the Hermitian conjugation. Thus they transform in the same way for all symmetry operations g :

$$g\mathbf{u} = \mathbf{u}\hat{D}(g), \quad (\text{C1a})$$

$$g\mathbf{v} = \mathbf{v}\hat{D}(g). \quad (\text{C1b})$$

Table VII. Compatibility chart of irreducible representations and basis functions for D_{3h} and C_{3h} point symmetry groups.

D_{3h}			C_{3h}	
Γ_7	ψ_1^7	$ -1/2\rangle$	Γ_8	ψ_1^7
	ψ_2^7	$ +1/2\rangle$	Γ_7	ψ_2^7
Γ_8	ψ_1^8	$ -1/2\rangle zS_z$	Γ_{10}	ψ_1^8
	ψ_2^8	$ +1/2\rangle zS_z$	Γ_9	ψ_2^8
Γ_9	ψ_1^9	$ -3/2\rangle$	Γ_{11}	ψ_1^9
	ψ_2^9	$ +3/2\rangle$	Γ_{12}	ψ_2^9

Using the coupling coefficients one can easily find operators belonging to Γ_2 representation

$$\hat{\tau}^{(2)} = \frac{i}{\sqrt{2}}(|1\rangle\langle 1| - |2\rangle\langle 2|) \propto \hat{\tau}_z, \quad (\text{C2})$$

and Γ_5 representation

$$\begin{aligned} \hat{\tau}_1^{(5)} &= -|1\rangle\langle 2| \propto (\hat{\tau}_x - i\hat{\tau}_y), \\ \hat{\tau}_2^{(5)} &= |2\rangle\langle 1| \propto -(\hat{\tau}_x + i\hat{\tau}_y). \end{aligned} \quad (\text{C3})$$

They are proportional to the components of the valley pseudospin operator $\hat{\tau}$, because they transform in the same way. Finally, the intervalley hyperfine interaction Hamiltonian can be written in a matrix form as

$$H_{\pm} = A_{\perp}(I_x\tau_x \pm I_y\tau_y) + A_{\parallel}\tau_z, \quad (\text{C4})$$

where A_{\perp} and A_{\parallel} are the constants and the different signs correspond to the different order of the basis func-

tions ($|1\rangle, |2\rangle$) or ($|2\rangle, |1\rangle$). This order is given in the last columns of Tables V and VI.

For Γ_9 representation of the wavefunctions the pseudovector operator $\hat{\tau}_z$ is given by Eq. (C2). The operator $\hat{\tau}_x$ belonging to Γ_3 representation has the form

$$\hat{\tau}^{(3)} = \frac{1}{2}(|1\rangle\langle 2| + |2\rangle\langle 1|) = \hat{\tau}_x. \quad (\text{C5})$$

Note, that there is a misprint in Ref. 61 in Table 67 with the corresponding coupling coefficients. Neglecting the noncollinear coupling between ΔI_z and τ_x , the symmetry allowed hyperfine interaction Hamiltonian is

$$\hat{H}_z = A_{\perp}I_z\hat{\tau}_z. \quad (\text{C6})$$

The bands and atoms relevant for this case are also given in Tables V and VI in the last column.

-
- [1] K. S. Novoselov, A. K. Geim, S. V. Morozov, D. Jiang, Y. Zhang, S. V. Dubonos, I. V. Grigorieva, and A. A. Firsov, "Electric field effect in atomically thin carbon films," *Science* **306**, 666 (2004).
- [2] K. S. Novoselov, D. Jiang, F. Schedin, T. J. Booth, V. V. Khotkevich, S. V. Morozov, and A. K. Geim, "Two-dimensional atomic crystals," *PNAS* **102**, 10451 (2005).
- [3] K. F. Mak, C. Lee, J. Hone, J. Shan, and T. F. Heinz, "Atomically Thin MoS_2 : A New Direct-Gap Semiconductor," *Phys. Rev. Lett.* **105**, 136805 (2010).
- [4] A. Splendiani, L. Sun, Y. Zhang, T. Li, J. Kim, C.-Y. Chim, G. Galli, and F. Wang, "Emerging photoluminescence in monolayer MoS_2 ," *Nano Lett.* **10**, 1271–1275 (2010).
- [5] G. Wang, A. Chernikov, M. M. Glazov, T. F. Heinz, X. Marie, T. Amand, and B. Urbaszek, "Colloquium: Excitons in atomically thin transition metal dichalcogenides," *Rev. Mod. Phys.* **90**, 021001 (2018).
- [6] A. Kormányos, G. Burkard, M. Gmitra, J. Fabian, V. Zolyomi, N. D. Drummond, and V. Fal'ko, " $\mathbf{k}\cdot\mathbf{p}$ theory for two-dimensional transition metal dichalcogenide semiconductors," *2D Materials* **2**, 022001 (2015).
- [7] G.-B. Liu, D. Xiao, Y. Yao, X. Xu, and W. Yao, "Electronic structures and theoretical modelling of two-dimensional group-VIB transition metal dichalcogenides," *Chem. Soc. Rev.* **44**, 2643 (2015).
- [8] D. Xiao, G.-B. Liu, W. Feng, X. Xu, and W. Yao, "Coupled Spin and Valley Physics in Monolayers of MoS_2 and Other Group-VI Dichalcogenides," *Phys. Rev. Lett.* **108**, 196802 (2012).
- [9] K. Kořmider, J. W. Gonzalez, and J. Fernandez-Rossier, "Large spin splitting in the conduction band of transition metal dichalcogenide monolayers," *Phys. Rev. B* **88**, 245436 (2013).
- [10] A. Molina-Sanchez, D. Sangalli, K. Hummer, A. Marini, and L. Wirtz, "Effect of spin-orbit interaction on the optical spectra of single-layer, double-layer, and bulk MoS_2 ," *Phys. Rev. B* **88**, 045412 (2013).
- [11] T. Cao, G. Wang, W. Han, H. Ye, C. Zhu, J. Shi, Q. Niu, P. Tan, E. Wang, B. Liu, and Feng J., "Valley-selective circular dichroism of monolayer molybdenum disulphide," *Nat. Commun.* **3**, 887 (2012).
- [12] S. Tarasenko, "2D materials: Valley currents controlled by light," *Nat. Nanotech.* **9**, 752 (2014).
- [13] T. Cheiwchanchamnangij and W. R. L. Lambrecht, "Quasiparticle band structure calculation of monolayer, bilayer, and bulk MoS_2 ," *Phys. Rev. B* **85**, 205302 (2012).
- [14] A. Ramasubramaniam, "Large excitonic effects in monolayers of molybdenum and tungsten dichalcogenides," *Phys. Rev. B* **86**, 115409 (2012).
- [15] D. Y. Qiu, F. H. da Jornada, and S. G. Louie, "Optical Spectrum of MoS_2 : Many-Body Effects and Diversity of Exciton States," *Phys. Rev. Lett.* **111**, 216805 (2013).
- [16] A. Chernikov, T. C. Berkelbach, H. M. Hill, A. Rigosi, Y. Li, O. B. Aslan, D. R. Reichman, M. S. Hybertsen, and T. F. Heinz, "Exciton Binding Energy and Nonhydrogenic Rydberg Series in Monolayer WS_2 ," *Phys. Rev. Lett.* **113**, 076802 (2014).
- [17] K. He, N. Kumar, L. Zhao, Z. Wang, K. F. Mak, H. Zhao, and J. Shan, "Tightly Bound Excitons in Monolayer WSe_2 ," *Phys. Rev. Lett.* **113**, 026803 (2014).
- [18] G. Wang, X. Marie, I. Gerber, T. Amand, D. Lagarde, L. Bouet, M. Vidal, A. Balocchi, and B. Urbaszek, "Giant Enhancement of the Optical Second-Harmonic Emission of WSe_2 Monolayers by Laser Excitation at Exciton Resonances," *Phys. Rev. Lett.* **114**, 097403 (2015).
- [19] Q. H. Wang, K. Kalantar-Zadeh, A. Kis, J. N. Coleman, and M. S. Strano, "Electronics and optoelectronics of two-dimensional transition metal dichalcogenides," *Nat. Nanotech.* **7**, 699 (2012).
- [20] S. Z. Butler, S. M. Hollen, L. Cao, Y. Cui, J. A. Gupta, H. R. Gutierrez, T. F. Heinz, S. S. Hong, J. Huang, A. F. Ismach, E. Johnston-Halperin, M. Kuno, V. V. Plashnitsa, R. D. Robinson, R. S. Ruoff, S. Salahuddin, J. Shan, L. Shi, M. G. Spencer, M. Terrones, W. Windl, and J. E. Goldberger, "Progress, Challenges,

- and Opportunities in Two-Dimensional Materials Beyond Graphene,” *ACS Nano* **7**, 2898–2926 (2013).
- [21] A. K. Geim and I. V. Grigorieva, “Van der Waals heterostructures,” *Nature* **499**, 419 (2013).
- [22] F. Xia, H. Wang, D. Xiao, M. Dubey, and A. Ramasubramanian, “Two-dimensional material nanophotonics,” *Nat. Phot.* **8**, 899 (2014).
- [23] X. Xu, W. Yao, D. Xiao, and T. F. Heinz, “Spin and pseudospins in layered transition metal dichalcogenides,” *Nat. Phys.* **10**, 343 (2014).
- [24] H. Yu, X. Cui, X. Xu, and W. Yao, “Valley excitons in two-dimensional semiconductors,” *Nat. Sci. Rev.* **2**, 57 (2015).
- [25] A. Castellanos-Gomez, “Why all the fuss about 2D semiconductors?” *Nat. Photon.* **10**, 202 (2016).
- [26] K. F. Mak and J. Shan, “Photonics and optoelectronics of 2D semiconductor transition metal dichalcogenides,” *Nat. Photon.* **10**, 216 (2016).
- [27] Gui-Bin L., Hongliang P., Yugui Y., and Wang Y., “Intervalley coupling by quantum dot confinement potentials in monolayer transition metal dichalcogenides,” *New J. Phys.* **16**, 105011 (2014).
- [28] Yue Wu, Qingjun Tong, Gui-Bin Liu, Hongyi Yu, and Wang Yao, “Spin-valley qubit in nanostructures of monolayer semiconductors: Optical control and hyperfine interaction,” *Phys. Rev. B* **93**, 045313 (2016).
- [29] C. Chakraborty, L. Kinnischtzke, K. M. Goodfellow, R. Beams, and A. N. Vamivakas, “Voltage-controlled quantum light from an atomically thin semiconductor,” *Nat. nanotech.* **10**, 507 (2015).
- [30] Y.-M. He, G. Clark, J. R. Schaibley, Y. He, M.-C. Chen, Y.-J. Wei, X. Ding, Q. Zhang, W. Yao, X. Xu, Lu C.-Y., and Pan J.-W., “Single quantum emitters in monolayer semiconductors,” *Nat. nanotech.* **10**, 497 (2015).
- [31] C. Chakraborty, L. Qiu, K. Konthasinghe, A. Mukherjee, S. Dhara, and N. Vamivakas, “3D Localized Trions in Monolayer WSe₂ in a Charge Tunable van der Waals Heterostructure,” *Nano Lett.* **18**, 2859–2863 (2018).
- [32] M. Atatüre, D. Englund, N. Vamivakas, S.-Y. Lee, and J. Wrachtrup, “Material platforms for spin-based photonic quantum technologies,” *Nat. Rev. Mat.* **3**, 38 (2018).
- [33] P. A. Lee and T. V. Ramakrishnan, “Disordered electronic systems,” *Rev. Mod. Phys.* **57**, 287 (1985).
- [34] B. Kramer and A. MacKinnon, “Localization: theory and experiment,” *Rep. Prog. Phys.* **56**, 1469 (1993).
- [35] F. Evers and A. D. Mirlin, “Anderson transitions,” *Rev. Mod. Phys.* **80**, 1355 (2008).
- [36] D. Gopalakrishnan, D. Damien, B. Li, H. Gullappalli, V. K. Pillai, P. M. Ajayan, and M. M. Shaijumon, “Electrochemical synthesis of luminescent MoS₂ quantum dots,” *Chem. Commun.* **51**, 6293 (2015).
- [37] Z. X. Gan, L. Z. Liu, H. Y. Wu, Y. L. Hao, Y. Shan, X. L. Wu, and P. K. Chu, “Quantum confinement effects across two-dimensional planes in MoS₂ quantum dots,” *Appl. Phys. Lett.* **106**, 233113 (2015).
- [38] S. Mukherjee, R. Maiti, A. K. Katiyar, S. Das, and S. K. Ray, “Novel colloidal MoS₂ quantum dot heterojunctions on silicon platforms for multifunctional optoelectronic devices,” *Sci. Rep.* **6**, 29016 (2016).
- [39] G. Wei, D. A. Czaplowski, E. J. Lenferink, T. K. Stanev, I. W. Jung, and N. P. Stern, “Size-tunable lateral confinement in monolayer semiconductors,” *Sci. Rep.* **7**, 3324 (2017).
- [40] A. Branny, G. Wang, S. Kumar, C. Robert, B. Lassagne, X. Marie, B. D. Gerardot, and B. Urbaszek, “Discrete quantum dot like emitters in monolayer MoSe₂: Spatial mapping, magneto-optics, and charge tuning,” *Appl. Phys. Lett.* **108**, 142101 (2016).
- [41] T. Li, M. Li, Y. Lin, H. Cai, Y. Wu, H. Ding, S. Zhao, N. Pan, and X. Wang, “Probing Exciton Complexes and Charge Distribution in Ink-slab-Like WSe₂ Homojunction,” *ACS Nano* **12**, 4959 (2018).
- [42] M. Koperski, K. Nogajewski, A. Arora, V. Cherkez, P. Mallet, J.-Y. Veullen, J. Marcus, P. Kossacki, and M. Potemski, “Single photon emitters in exfoliated WSe₂ structures,” *Nat. nanotech.* **10**, 503 (2015).
- [43] A. Srivastava, M. Sidler, A. V. Allain, D. S. Lembke, A. Kis, and A. Imamoglu, “Optically active quantum dots in monolayer WSe₂,” *Nat. nanotech.* **10**, 491 (2015).
- [44] B. Ganchev, N. Drummond, I. Aleiner, and V. Fal’ko, “Three-Particle Complexes in Two-Dimensional Semiconductors,” *Phys. Rev. Lett.* **114**, 107401 (2015).
- [45] L. Yang, W. Chen, K. M. McCreary, B. T. Jonker, J. Lou, and S. A. Crooker, “Spin Coherence and Dephasing of Localized Electrons in Monolayer MoS₂,” *Nano Lett.* **15**, 8250–8254 (2015).
- [46] L. Yang, N. A. Sinitsyn, W. Chen, J. Yuan, J. Zhang, J. Lou, and S. A. Crooker, “Long-lived nanosecond spin relaxation and spin coherence of electrons in monolayer MoS₂ and WS₂,” *Nat. Phys.* **11**, 830 (2015).
- [47] E. J. McCormick, M. J. Newburger, Y. K. Luo, K. M. McCreary, S. Singh, I. B. Martin, E. J. Cichewicz Jr, B. T. Jonker, and R. K. Kawakami, “Imaging spin dynamics in monolayer WS₂ by time-resolved Kerr rotation microscopy,” *2D Materials* **5**, 011010 (2018).
- [48] W.-T. Hsu, Y.-L. Chen, C.-H. Chen, P.-S. Liu, T.-H. Hou, L.-J. Li, and W.-H. Chang, “Optically initialized robust valley-polarized holes in monolayer WSe₂,” *Nat. Commun.* **6**, 8963 (2015).
- [49] X. Song, S. Xie, K. Kang, J. Park, and V. Sih, “Long-Lived Hole Spin/Valley Polarization Probed by Kerr Rotation in Monolayer WSe₂,” *Nano Lett.* **16**, 5010 (2016).
- [50] P. Dey, L. Yang, C. Robert, G. Wang, B. Urbaszek, X. Marie, and S. A. Crooker, “Gate-Controlled Spin-Valley Locking of Resident Carriers in WSe₂ Monolayers,” *Phys. Rev. Lett.* **119**, 137401 (2017).
- [51] M. M. Glazov, *Electron & Nuclear Spin Dynamics in Semiconductor Nanostructures* (Oxford University Press, 2018).
- [52] W. A. Coish and J. Baugh, “Nuclear spins in nanostructures,” *physica status solidi (b)* **246**, 2203 (2009).
- [53] G. Sharma, S. E. Economou, and E. Barnes, “Interplay of valley polarization and dynamic nuclear polarization in 2D transition metal dichalcogenides,” *Phys. Rev. B* **96**, 125201 (2017).
- [54] S. A. Tarasenko and G. Burkard, “Limitation of electron mobility from hyperfine interaction in ultraclean quantum wells and topological insulators,” *Phys. Rev. B* **94**, 045309 (2016).
- [55] S. Fang, D. R. Kuate, S. N. Shirodkar, S. Lieu, G. A. Tritsarlis, and E. Kaxiras, “*Ab initio* tight-binding hamiltonian for transition metal dichalcogenides,” *Phys. Rev. B* **92**, 205108 (2015).
- [56] L. D. Landau and E. M. Lifshitz, *Quantum Mechanics: Non-Relativistic Theory (vol. 3)* (Butterworth-Heinemann, Oxford, 1977).
- [57] M. V. Durnev and M. M. Glazov, “Excitons and trions

- in two-dimensional semiconductors based on transition metal dichalcogenides,” *Phys. Usp* **61** (2018).
- [58] K. S. Novoselov, A. Mishchenko, A. Carvalho, and A. H. Castro Neto, “2D materials and van der Waals heterostructures,” *Science* **353** (2016).
- [59] J. R. Schaibley, H. Yu, G. Clark, P. Rivera, J. S. Ross, K. L. Seyler, W. Yao, and X. Xu, “Valleytronics in 2D materials,” *Nat. Rev. Mat.* **1**, 16055 (2016).
- [60] G. Wang, C. Robert, M. M. Glazov, F. Cadiz, E. Courtade, T. Amand, D. Lagarde, T. Taniguchi, K. Watanabe, B. Urbaszek, and X. Marie, “In-Plane Propagation of Light in Transition Metal Dichalcogenide Monolayers: Optical Selection Rules,” *Phys. Rev. Lett.* **119**, 047401 (2017).
- [61] George F. Koster, Robert G. Wheeler, John O. Dimmock, and Hermann Statz, *Properties of the thirty-two point groups* (MIT Press, 1963).
- [62] A. A. Mitioglu, P. Plochocka, Á. Granados del Aguila, P. C. M. Christianen, G. Deligeorgis, S. Anghel, L. Kulyuk, and D. K. Maude, “Optical Investigation of Monolayer and Bulk Tungsten Diselenide (WSe₂) in High Magnetic Fields,” *Nano Lett.* **15**, 4387 (2015).
- [63] A. Arora, R. Schmidt, R. Schneider, M. R. Molas, I. Breslavetz, M. Potemski, and R. Bratschitsch, “Valley Zeeman Splitting and Valley Polarization of Neutral and Charged Excitons in Monolayer MoTe₂ at High Magnetic Fields,” *Nano Lett.* **16**, 3624 (2016).
- [64] B. Urbaszek, X. Marie, T. Amand, O. Krebs, P. Voisin, P. Maletinsky, A. Högele, and A. Imamoglu, “Nuclear spin physics in quantum dots: An optical investigation,” *Rev. Mod. Phys.* **85**, 79–133 (2013).
- [65] E. I. Grncharova and V. I. Perel, “Relaxation of Nuclear Spins Interacting With Holes in Semiconductors,” *Sov. Phys. Semicond.* **11**, 997 (1977).
- [66] D. V. Rybkovskiy, I. C. Gerber, and M. V. Durnev, “Atomically inspired $k \cdot p$ approach and valley Zeeman effect in transition metal dichalcogenide monolayers,” *Phys. Rev. B* **95**, 155406 (2017).
- [67] M. Vidal, M. V. Durnev, L. Bouet, T. Amand, M. M. Glazov, E. L. Ivchenko, P. Zhou, G. Wang, T. Mano, T. Kuroda, X. Marie, K. Sakoda, and B. Urbaszek, “Hyperfine coupling of hole and nuclear spins in symmetric (111)-grown GaAs quantum dots,” *Phys. Rev. B* **94**, 121302 (2016).
- [68] The last term in Eq. (9) being a part of the dipole-dipole interaction can change the electron orbital momentum m_z by ± 2 , but simultaneously the electron spin s_z changes by ∓ 1 , so the total angular momentum f_z can not be changed by more than 1, in agreement with the spherical symmetry of the Hamiltonian (9).
- [69] H. Overhof and U. Gerstmann, “Ab Initio Calculation of Hyperfine and Superhyperfine Interactions for Shallow Donors in Semiconductors,” *Phys. Rev. Lett.* **92**, 087602 (2004).
- [70] R. Benchamekh, F. Raouafi, J. Even, F. Ben Cheikh Larbi, P. Voisin, and J.-M. Jancu, “Microscopic electronic wave function and interactions between quasiparticles in empirical tight-binding theory,” *Phys. Rev. B* **91**, 045118 (2015).
- [71] A.K. Koh and D.J. Miller, “Hyperfine coupling constants and atomic parameters for electron paramagnetic resonance data,” *Atomic Data and Nuclear Data Tables* **33**, 235 (1985).
- [72] S. Adachi, “Properties of Group-IV, III-V and II-VI Semiconductors,” England: John Wiley & Sons Ltd , 373 (2005).
- [73] E. A. Chekhovich, M. M. Glazov, A. B. Krysa, M. Hopkinson, P. Senellart, A. Lemaitre, M. S. Skolnick, and A. I. Tartakovskii, “Element-sensitive measurement of the hole-nuclear spin interaction in quantum dots,” *Nat. Phys.* **9**, 74 (2013).
- [74] Ph. Glasenapp, D. S. Smirnov, A. Greilich, J. Hackmann, M. M. Glazov, F. B. Anders, and M. Bayer, “Spin noise of electrons and holes in (In,Ga)As quantum dots: Experiment and theory,” *Phys. Rev. B* **93**, 205429 (2016).
- [75] D. Paget, G. Lampel, B. Sapoval, and V. I. Safarov, “Low field electron-nuclear spin coupling in gallium arsenide under optical pumping conditions,” *Phys. Rev. B* **15**, 5780 (1977).
- [76] E. A. Chekhovich, A. Ulhaq, E. Zallo, F. Ding, O. G. Schmidt, and M. S. Skolnick, “Measurement of the spin temperature of optically cooled nuclei and GaAs hyperfine constants in GaAs/AlGaAs quantum dots,” *Nat. mat.* **16**, 982 (2017).
- [77] I. A. Merkulov, Al. L. Efros, and M. Rosen, “Electron spin relaxation by nuclei in semiconductor quantum dots,” *Phys. Rev. B* **65**, 205309 (2002).
- [78] A. V. Khaetskii and Y. V. Nazarov, “Spin-flip transitions between Zeeman sublevels in semiconductor quantum dots,” *Phys. Rev. B* **64**, 125316 (2001).
- [79] L. M. Woods, T. L. Reinecke, and Y. Lyanda-Geller, “Spin relaxation in quantum dots,” *Phys. Rev. B* **66**, 161318 (2002).
- [80] G. Kioseoglou, A. T. Hanbicki, M. Currie, A. L. Friedman, D. Gunlycke, and B. T. Jonker, “Valley polarization and intervalley scattering in monolayer MoS₂,” *Appl. Phys. Lett.* **101**, 221907 (2012).
- [81] L. C. Camenzind, L. Yu, P. Stano, J. D. Zimmerman, A. C. Gossard, D. Loss, and D. M. Zumbühl, “Hyperfine-phonon spin relaxation in a single-electron GaAs quantum dot,” *Nat. commun.* **9**, 3454 (2018).
- [82] Z. Liu, M. O. Nestoklon, J. L. Cheng, E. L. Ivchenko, and M. W. Wu, “Spin-dependent intravalley and intervalley electron-phonon scatterings in germanium,” *Phys. Solid State* **55**, 1619–1634 (2013).
- [83] A. J. Pearce and G. Burkard, “Electron spin relaxation in a transition-metal dichalcogenide quantum dot,” *2D Materials* **4**, 025114 (2017).
- [84] G. Széchenyi, L. Chirolli, and A. Pályi, “Impurity-assisted electric control of spin-valley qubits in monolayer MoS₂,” *2D Materials* **5**, 035004 (2018).
- [85] V. Baltz, A. Manchon, M. Tsoi, T. Moriyama, T. Ono, and Y. Tserkovnyak, “Antiferromagnetic spintronics,” *Rev. Mod. Phys.* **90**, 015005 (2018).
- [86] M. I. Dyakonov and V. I. Perel, “Dynamic self-polarization of nuclei in solids,” *JETP Lett.* **16**, 398 (1972).
- [87] V. L. Korenev, “Dynamic self-polarization of nuclei in low-dimensional systems,” *JETP Lett.* **70**, 129 (1999).
- [88] I. A. Merkulov, “Formation of a nuclear spin polaron under optical orientation in GaAs-type semiconductors,” *Phys. Solid State* **40**, 930 (1998).
- [89] R. Oulton, A. Greilich, S. Yu. Verbin, R. V. Cherbunin, T. Auer, D. R. Yakovlev, M. Bayer, I. A. Merkulov, V. Stavarache, D. Reuter, and A. D. Wieck, “Subsecond Spin Relaxation Times in Quantum Dots at Zero Applied Magnetic Field Due to a Strong Electron-Nuclear Interaction,” *Phys. Rev. Lett.* **98**, 107401 (2007).

- [90] W. Jiang, P. Upadhyaya, W. Zhang, G. Yu, M. B. Jungfleisch, F. Y. Fradin, J. E. Pearson, Y. Tserkovnyak, K. L. Wang, O. Heinonen, S. G. E. te Velthuis, and A. Hoffmann, “Blowing magnetic skyrmion bubbles,” *Science* **349**, 283 (2015).
- [91] W. Jiang, X. Zhang, G. Yu, W. Zhang, X. Wang, M. B. Jungfleisch, J. E. Pearson, X. Cheng, O. Heinonen, K. L. Wang, Y. Zhou, A. Hoffmann, and S. G. E. te Velthuis, “Direct observation of the skyrmion Hall effect,” *Nat. Phys.* **13**, 162 (2017).
- [92] G. L. Bir and G. E. Pikus, *Symmetry and deformation effects in semiconductors (in Russian)* (Moscow (Nauka), 1972).